Journal of Optoelectronics and Advanced Materials, Vol. 3, No. 4, December 2001, p. 885 - 895

NANOPARTICLE LAYERS OF CdSe IN VARIOUS MULTILAYER STRUCTURES

D. Nesheva

Institute of Solid State Physics, Bulgarian Academy of Sciences, Sofia 1784, Bulgaria

In this article, main results on preparation of CdSe nanoparticle layers sandwiched between oxide or chalcogenide amorphous films are summarized. Multilayer structures are deposited by thermal evaporation in vacuum, in which CdSe sublayer thickness varies between 1 and 10 nm, while the sublayers from the second material are either equal or 20 times greater then CdSe sublayers. High-resolution electron microscopy results prove the formation of CdSe nanoparticle layers, which are continuous at equal sublayer thicknesses. In the second case CdSe layers are discontinuous; particles with nearly spherical form are observed, whose spatial distribution followed the surface morphology of the film below. The mechanism of semiconductor nanoparticle formation during nonepitaxial layer growth is discussed. It is shown that nanoparticle size distribution in these films is slightly narrow than in semiconductor doped glasses. A significant difference is observed in the nanoparticle size determined by electron microscopy and high angle X-ray diffraction, which is ascribed to appreciable CdSe lattice deformations. Investigations on carrier transport in SiO_x-CdSe and GeS_2-CdSe multilayers structures are also described. It is assumed that percolation paths for carriers exist in both continuous and discontinuous CdSe nanoparticle layers and potential barriers for electrons existing at the CdSe-CdSe interface control carrier transport.

(Received June 6, 2001; accepted December 5, 2001)

Keywords: Thermal evaporation, Multilayer structures, CdSe nanoparticles

1. Introduction

Over the past two decades there has been rapidly growing interest in the preparation of semiconductor nanometer-sized particles. The development of various techniques for growing nanocrystals (NCs) from a great variety of semiconductor materials (CdSe, CdS, TiO_2, Si, Ge, GaAs, CuBr, CuCl etc.) has allowed intensive studies on their linear, non-linear and electro-optical properties [1-5]. From fundamental point of view this enhanced interest is justified because NCs essentially constitute intermediate systems between solids and isolated molecules. On the other hand, this interest is related to a great variety of potential applications in optical and optoelectronic devices, solar cells etc. Bulk composites of Cd chalcogenide semiconductors ($CdSe_xS_{1-x}$) and silicate glasses (so called doped glasses, which are widely used as color filters) have also been focus of intensive research. These composites are a good subject for studying quantum size effects in semiconductor quantum dots [6,7]. Moreover, they demonstrate a high and fast optical nonlinearity [8-10] interesting for signal processing or designing of optical communication systems. Photo- and electroluminescence of CdSe nanocrystals [11,12] is interesting for the practice with the observed change in the color of the emission when changing the nanocrystallite size.

Semiconductor doped glasses are prepared by a long-time co-melting of the semiconductor components with some silicate glass at high temperatures ($T\approx1500K$) followed by nanocrystallite growth at temperatures T>900K for several to one hundred hours. Thin film counterparts of doped glasses have also been produced [2,13], in which the first step is co-sputtering of SiO_2 and II-VI semiconductor and the second one is nanocrystallite growth at temperatures T>900K. A variety of other techniques, such as molecular and atomic layer epitaxy, colloidal methods, electrodeposition etc.[14,15 and references therein], have been applied for preparation of thin film systems comprising II-VI nanoparticles. The most popular mechanism of semiconductor nanoparticle formation is the Stranski-Krastanow self-organized epitaxial growth in strained systems, which takes place on the

smooth surface of a crystalline material. It has also been shown [16-18] that a nonepitaxial self-organized formation of metal nanoclusters is possible on the surface of amorphous thin films (a-Si:H, SiO_x, Al_2O_3) when physical evaporation, sputtering or glow-discharge techniques were used. Multilayers consisting of planes of metal clusters separated by continuous amorphous films have been produced by means of a sequential deposition of metal and insulator sublayers. The partial wetting character of the metal with respect to the other material [16] or filling up of the existing valleys of the amorphous film surface [17] have been considered as possible mechanisms for the formation of metal nanoclusters. An intentionally created surface roughness on a ZnSe crystalline surface has also been used [19] for obtaining ZnCdSe quantum dots but the size distribution of those dots is rather wide.

Thermal post-treatment of regular amorphous multilayers (MLs) is another approach for the preparation of nanocrystalline materials [20,21]. The main advantage of this approach is the possibility for a precise control of the sublayer thickness during the ML deposition procedure. This makes possible fabrication of semiconductor NCs with desired sizes in MLs having sublayer thickness of a few nanometers. Moreover, the great flexibility of amorphous materials strongly reduces the requirements for matching the lattice constants of the constituent materials and makes possible application of a great variety of materials in the fabrication of amorphous multilayers. Besides, regular amorphous MLs have been prepared by a variety of rather simple and cheap set-ups, as compared to those applied for fabrication of crystalline MLs. Chalcogenide and a-Si:H based MLs have been annealed for various times at temperatures around and above the crystallization temperature of the constituent material having lower crystallization temperature [20,22-29]. Laser beam crystallization under cw or pulse exposure has also been applied [30,31].

In this article, our recent results on the production of continuous and ‘island’ type CdSe nanoparticle layers by means of a multilayer approach are reviewed. Amorphous SiO_x or GeS_2 is used as the second constituent material in the multilayer structures. The mechanism of nanoparticle formation as well as carrier transport in CdSe nanoparticle layers are discussed.

2. Fabrication of CdSe nanoparticle layers in multilayer structures

2.1 Regular multilayers

Experiments on preparation of amorphous MLs based on a-Si:H showed [32] that layers deposited in a step-by-step manner were smoother than those made in one step. Taking into account this result, we developed two techniques for fabrication of regular chalcogenide amorphous MLs based on thermal evaporation [33] and laser beam sputtering [34,35] of materials. Amorphous chalcogenide MLs of *pnpn* type (Se/CdSe and $Se_{100-x}Te_x$/CdSe) and *pp+pp+* type (Se/$Se_{100-x}Te_x$) were deposited by means of these deposition techniques. Periodicity and interface quality of Se/CdSe and $Se_{100-x}Te_x$/CdSe amorphous MLs, deposited using the step-by-step approach, were studied by small-angle *X*-ray diffraction [24,33,36]. The results obtained showed [36] that sublayers of the MLs are continuous and the ML periodicity keeps dawn to a sublayer thickness of 2.5 nm. A sinusoidal composition change has been suggested for sublayer thicknesses < 2.5 nm. Values between 0.6 and 1.6 nm were determined [24,33] for the effective interface thickness of the as-deposited MLs, which confirm the hint for abrupt interfaces in chalcogenide amorphous MLs, prepared with the step-by-step approach. The small and high angle X-ray diffraction spectra of Se/CdSe amorphous MLs, annealed at various temperatures for 18 hours showed [27] that a prolong annealing at 363 K caused crystallization in Se sublayers. However the periodic structure of these MLs vanished after annealing at 333 K. On the other hand, the small-angle *X*-ray diffraction and high resolution electron microscopy studies on Ge:H/GeN_x amorphous MLs indicated [20] that the multilayer periodisity was preserved after the crystallization of a-Ge:H sublayers. A similar result has also been obtained [29,31] for a-Si:H based amorphous MLs. Hence, one may conclude that the crystallization of one kind of sublayers of an amorphous ML may not destroy its artificial periodicity if the structure of the second constituent material is enough rigid to restrict the crystal growth. Keeping in mind this conclusion, we applied the developed thermal evaporation technique for preparation of regular multilayer structures of SiO_x-CdSe (further referred to as SiO_x/CdSe MLs). It was assumed that SiO_x films would by rigid enough to prevent the periodisity breakdown during ML annealing for 60 to 90 min at 673 K in air or argon. This annealing was carried out in order to improve crystallinity of CdSe sublayers. MLs from GeS_2/CdSe were also produced, which were not annealed in order to avoid material alloying at interfaces.

The SiO_x/CdSe and GeS_2/CdSe MLs were produced in a vacuum chamber at residual pressure of about 1.10^3 and 3.10^{-4} Pa, respectively. A consecutive evaporation was carried out from two independent tantalum crucibles mounted as far as possible apart from each other (Fig. 1). Powered CdSe (Merck, Suprapur) and preliminary synthesized glassy GeS_2 *or* commercial SiO were used as source materials. Jena glass (for CdSe) and molibdenum (for SiO and GeS_2) cylinders, not deliberately heated, were installed above the sources in order to ensure evaporation in a quasi-closed volume. The sublayer thickness and deposition rate of both materials were measured during deposition by two preliminary calibrated monitors MIKI-FFV, whose quartz crystal heads were fixed above the respective source. In all MLs sublayer thickness was varied between 2.5 and 10 nm and both constituent sublayers had approximately equal thicknesses. During the deposition of each sublayer of the regular SiO_x-CdSe and GeS_2-CdSe multilayer structures Corning 7059 glass and c-Si substrates, kept at room temperature, were rotated at a rate varying between 8 and 30 turns/min. They spent over the source only 1/12 part of the turn time and, thus, ten or more 'layers', with a nominal thickness of ~0.1-0.25 nm in each step, form the respective sublayer in MLs. The substrates were stopped at the greatest possible distance from both sources at the moment the evaporation source was changed. Fig.2 displays a small angle X-ray diffraction pattern of an annealed SiO_x/CdSe ML [37]. It is seen that this ML exhibits a very good periodicity. The structure of CdSe nanoparticle layers in SiO_x/CdSe MLs annealed at 673K for 60 min was investigated by high resolution electron microscopy (HREM). The cross section electron micrograph showed [38] that CdSe sublayers are continuous; they consist of randomly oriented nanocrystals. The size of CdSe nanocrystals along the ML axis is equal to the sublayer thickness.

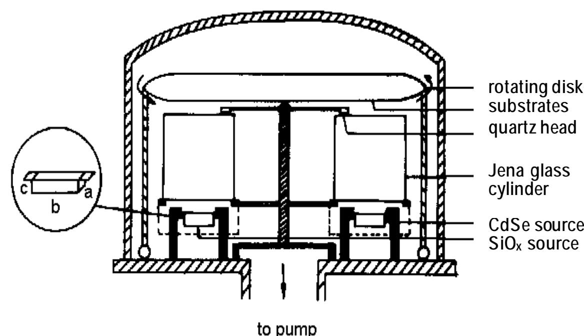

Fig. 1. The vacuum chamber used for preparation of CdSe nanoparticle layers in various multilayer structures. The tantalum crucibles have linear dimensions of a=1 cm, b=2 cm and c=1 cm. Substrates were mounted on the bottom of the rotating disk.

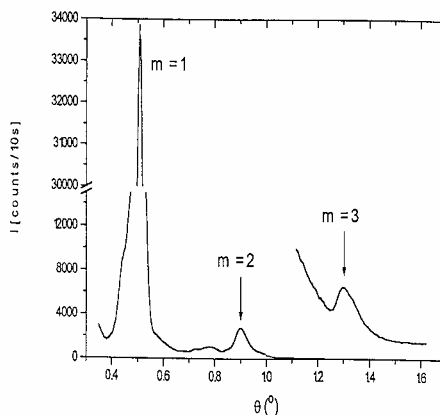

Fig. 2. Small-angle X ray diffracton pattern of SiO_x/CdSe multilayer structure with d_{CdSe}= 4.0 nm and 20 periods, annealed at 673 K for 60 min [37].

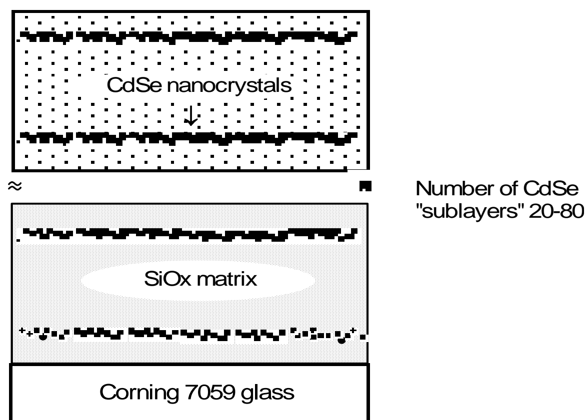

Fig. 3. Schematic presentation of SiO_x-CdSe composite films in which the nominal CdSe layer thickness d_{CdSe}. varies between 1 and 6 nm and d_{SiOx}=20 d_{CdSe}.

2.2. Composite films

It is known that during the nonepitaxial growth of thin films the roughness of the top surface of these films varies with the deposition techniques. In case of thermal evaporation of materials this amplitude is ~ $d^{1/2}$ (*d* –film thickness) [39]. Hence, one can expect that in a two-layer structure in which the first layer is relatively thick (with a 'rough' surface) and the second one is super thin (a few nanometers), the latter may be 'island' type. Keeping in mind this expectation, a second type not regular multilayer structures (further referred to as composite films, CFs) of consequently deposited SiO_x (or GeS_2) and CdSe films were fabricated (Fig.3) by modifying technique applied for vacuum thermal deposition of regular multilayers. In the modified approach SiO_x (GeS_2) sublayers (20-120 nm thick) of the composite films were deposited in one-step procedure and, besides, in all samples the SiO_x (GeS_2) thickness (d_{SiOx}) was 20 times greater than the CdSe one (d_{CdSe}). Samples of each system were annealed for 60-90 min at 673 K. The SiO_x-CdSe composite films were annealed in air or argon while the GeS_2-CdSe ones were annealed only in argon. More details on preparation conditions of MLs and CFs can be found in our previous articles [3,40,41].
High-resolution electron microscopy was performed (by means of a JEM 4000 EX operating at 400kV) [41,42] to prove the growth of 'island' type CdSe nanoparticle sublayers on top of the relatively thick SiO_x (x≈1.5) or GeS_2 ones. Cross-sectional electron micrographs of SiO_x-CdSe and GeS_2-CdSe three layer structures are shown in Figs.4a and 4b. CdSe particles are revealed in both systems, which are not disposed in a plane. Their spatial distribution follows the surface morphology of the SiO_x or GeS_2 films, respectively. CdSe nanoparticles are partly isolated and partly in contact among each other. The higher magnification has shown (Fig.5a [41]) that the nanoparticles exhibit nearly spherical shapes. In as-deposited samples having CdSe nominal thickness d_{CdSe}≥2 nm the particles are crystalline and their lattice is oriented randomly. The annealing improves crystallinity of the nanoparticles (Fig.5b). Neither as-deposited nor annealed samples having CdSe nominal thickness d_{CdSe}=1 nm exhibit good crystallinity. This is most likely due to the strong disorder effect of the large nanoparticle surface.

3. Average size of CdSe nanoparticles and size distribution

In order to determine the average size of CdSe microcrystals in annealed SiO_x/CdSe MLs and CFs, high angle X-ray diffraction were performed on samples having various nominal sublayer thicknesses as well as on a Corning 7059 substrate. It has been shown [43] that X-ray diffraction from the substrate in the (110) band region is marginal and should not appreciably change the shape of the band. In order to calculate the average nanocrystallite diameter, d_a, the Scherrer's equation

$$d_a = \lambda / \delta 2\Theta \cos\Theta \tag{1}$$

was employed to the (110) band. In this equation Θ and $\delta 2\Theta$ are the position and full width at half maximum of the band. Values , d_a = 1.5 and 2 nm have been obtained for the nanocrystal size in the samples having nominal CdSe sublayer thickness of 1 nm and 2 nm, respectively, which are very close to the nominal thickness of CdSe sublayers. The average CdSe nanoparticle size has also been determined [41] from cross section electron micrographs of as-deposited and annealed SiO_x(20 nm)/CdSe(1 nm)/SiO_x(20nm) and SiO_x(40 nm)/CdSe(2 nm)/SiO_x(20nm) three layer structures at high magnification (x500 000). The values of ~2.5 nm and ~4.8 nm obtained are more than two times greater than the ones calculated from the X-ray diffraction spectra. A similar result has been obtained for the SiO_x/CdSe MLs.

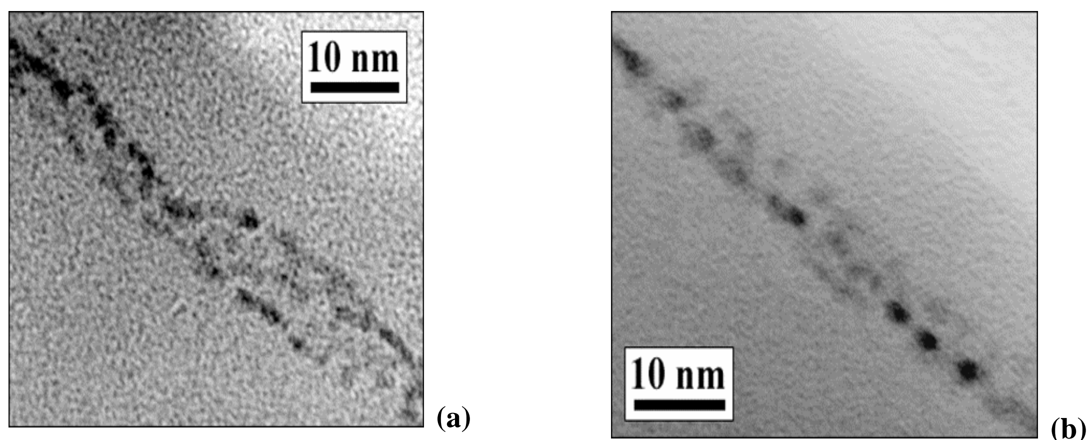

Fig. 4. Cross-section view of as-deposited three layer structures at low magnification: (a)-SiO_x(40 nm)/CdSe(2 nm)/SiO_x(20nm) and (b) - GeS_2(40 nm)/CdSe(2 nm)/GeS_2(20nm).

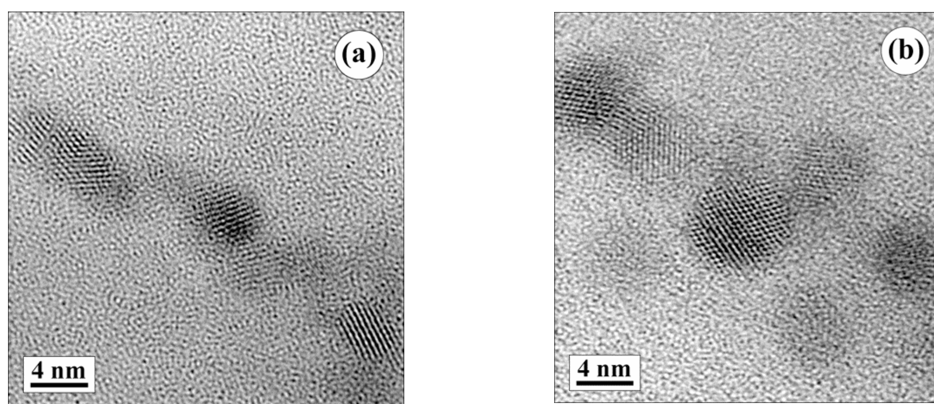

Fig. 5. Cross section view of as-deposited (a) and annealed (b) SiO_x(40 nm) /CdSe(2 nm)/ SiO_x(20nm) three layer structure. CdSe sublayer consists of nanoparticles of nearly spherical shape, which follow the surface morphology of the SiO_x film [41].

In order to explain the observed discrepancy one should take into account that the full width at half maximum of X-ray diffraction peaks depends not only on the NC size but also on existing microstrains and deformations in the NC network [44]. We assumed a high level of microstrains in the CdSe nanocrystals, even in samples annealed at 673K. In order to find some corroboration for this suggestion, the approximate levels of the microstrains in SiO_x/CdSe MLs were estimated assuming that both CdSe NC size and strain (ε) distributions are Gaussian. The relation [44]

$$(\delta 2\theta \cos\theta/\lambda)^2 = 1/d_a^2 + 16\varepsilon^2(\sin\theta/\lambda)^2 \quad (2)$$

was used, in which the respective average diameters were assumed to be equal to the CdSe sublayer thickness. Values of around 20×10^{-3} and 28×10^{-3} have been obtained for nanocrystals having $d_a=d_{CdSe}$=10.0 and 5.0 nm, respectively. They are close to the values of 20-22.10^{-3} calculated [45] for the CdSe layers of a free-standing CdS/CdSe superlattices with layers of equal thickness. A value of $\varepsilon \approx 49\times10^{-3}$ has been determined for NCs having d_a=3.0 nm, which indicates that the level of microstrains rises with decreasing NC size. Therefore, we accept that in SiO_x/CdSe MLs the NC size is equal to the respective CdSe sublayer thickness.

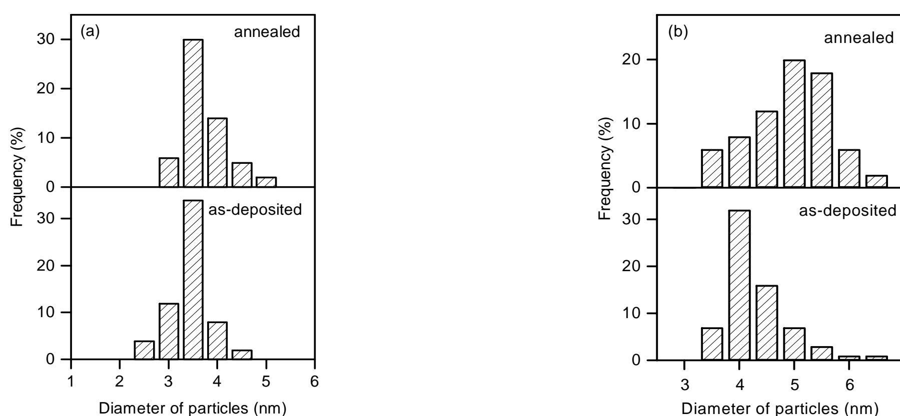

Fig. 6. Size distribution of CdSe nanoparticles in as-deposited and annealed: (a)-SiO_x(20nm) / CdSe(1nm) / SiO_x(20 nm) and (b) - SiO_x(40 nm)/CdSe(2 nm)/SiO_x(20 nm) structures [41].

The size distribution of CdSe nanoparticles in as-deposited and annealed SiO_x-CdSe composite samples deduced from HREM results is shown in Fig.6a and 6b, respectively. As mentioned above, in as deposited structures the average nanocluster size is more than two times greater than the respective nominal CdSe layer thickness. After annealing a well expressed increase of the average diameter is observed, accompanied by a slight increase in the width of size distribution. All nanoparticle size distributions shown in Fig 6a and 6b were fitted to Gaussian and values of ~0.13 and ~0.14 have obtained for σ/d_a ratio in as-deposited and annealed SiO_x(20 nm)/CdSe(1 nm)/SiO_x(20 nm) structures, respectively (here σ is half width at half maximum of the size distribution). In both as-deposited and annealed SiO_x(40 nm)/CdSe(2 nm)/SiO_x(20 nm) structure $\sigma/d_a \approx 0.19$. This nanocrystal size-distribution is slightly narrower than those reported for CdS [46] and Ge [47] nanocrystals, which were grown in thin SiO_2 matrix during the annealing of thin amorphous films of CdS-doped SiO_2 and $Si_{1-x}O_xGe_y$, respectively.

4. Mechanism of CdSe nanoparticle formation

The Stranski-Krastanow self-organized epitaxial growth in strained systems, which takes place on the smooth surface of crystalline materials, could not be invoked to explain nanoparticle formation on a ‘rough’ surface. The sequential vapor deposition of two materials, which we use for preparation of CdSe nanocluster layers has been also applied for nonepitaxial growth of nanosized metallic clusters embedded in insulating matrix. In this approach both kinds of films have approximately equal thickness of a few nanometers. The partial wetting character of Ga with respect to SiO_x has been considered [16] as responsible for the formation of liquid Ga nanoclusters on the surface of SiO_x thin films. It has also assumed [17] that the existing valleys of the thin film a-Si:H surface support clustering of Mo, W. Also, the three dimensional growth of most of the transition and noble metals on insulator has been attributed [48] to the large difference of surface energies. The cross-sectional electron micrograph of SiO_x/CdSe multilayers shows that when in the SiO_x/Ga MLs

the metal is replaced by a few nanometer semiconductor film, the latter is continuous rather than 'island' type. However when the SiO_x surface is 'rough', CdSe particle formation takes place, as the spatial distribution of nanoparticles follows the surface morphology of the SiO_x and GeS_2 films. This implies that different mechanisms should be responsible for the metal and semiconductor nanoparticle formation. Obviously, neither the assumption for difference of surface energies nor filling up of the existing valleys (suggested for the Mo and W cluster formation on the a-Si:H surface [17]) could explain our observations. Besides, one could not expect the same partial wetting character of CdSe with respect to SiO_x and GeS_2.

It is known [39] that at the first stage of thin film deposition on a rough surface an embryo formation takes place, which depends on the temperature and chemical nature of the substrate surface. Besides the curvature and stress at a rough or even disordered surface strongly affect reaction rates at a solid interface as they create different environments at different reaction sites [49]. The results of HREM and X-ray diffraction measurements showed that the surface of SiO_x sublayers in the regular SiO_x/CdSe multilayer structure is smooth, which allows us to assume that a homogeneous embryo formation occurs at the first stage of CdSe deposition. New embryo formation, gradual increase in the nanoparticle size and coalescence can be expected at the second stage. However in the composition films we observed a spatial distribution of the CdSe clusters which follows the surface morphology of the SiO_x and GeS_2 films. This observation indicates the surface roughness plays important role in the nanoparticle formation. Therefore we assume that, independently on the chemical nature of the surface, at the very beginning of CdSe deposition embryos are formed at those surface positions at which the curvature and lattice stress are the greatest. The relatively narrow nanocluster size distribution indicates that, most likely, further CdSe deposition does not create new embryos but leads only to an increase in the nanocluster size. Thus, at low substrate temperatures and thickness ratio of d_{SiO}/d_{CdSe} = 20 the surface roughness of the 'matrix' layers is great enough to ensure formation of quasi-isolated CdSe nanoclusters. The suggested mechanism of self-organized nanocluster formation on a rough surface implies that the multilayer approach described may be applied for fabrication of semiconductor nanoparticle layers in various matrices as well as regular amorphous/nanocrystaline multilayer structures from various materials.

Table 1. Experimental parameters for SiO_x and CdSe single layers and SiO_x- CdSe multilayer structures prepared at the same deposition conditions.

Nominal CdSe sublayer thickness d_w (nm)	Regular multilayer structures			Composite films	
	Dark conductivity σ_d (S/cm)	Dark current activation energy, E_{ad} (eV)	Photo-current activation energy, E_{ap} (eV)	Dark conductivity σ_d (S/cm)	Dark current activation energy, E_{ad} (eV)
SiO_x (1000)	$5x10^{-12}$	0.55			
CdSe (200)	$2x10^{-7}$	0.55			
10.0	$2.5x10^{-9}$	0.68	0.13		
6.0				$2x10^{-4}$	0.40
5.0	10^{-9}	0.62	<0.1		
4.0	$8x10^{-11}$	0.80	0.23	$2x10^{-4}$	0.40
3.5	$5x10^{-11}$	0.77	0.13		
3.0	10^{-10}	0.63		$3x10^{-7}$	0.50
2.5	$5x10^{-11}$	0.83	0.23		
2.0				$1x10^{-9}$	0.87

5. Carrier transport in multilayers and composite films

The mechanism of carrier transport in a poly- and nanocrystalline layer strongly affects the temperature dependence of the dark conductivity. Parallel dark current temperature measurements have been carried out on SiO_x/CdSe, GeS_2/CdSe multilayers and composite films having varying nominal CdSe sublayer thicknesses and, for comparison, on SiO_x, GeS_2 and CdSe single layers prepared at the same deposition conditions [50]. Dark current activation energy E_{ad} was determined in

all samples from the slope of the high temperature part of the curves in accordance with the relation

$$I_d=I_{do}\exp(-E_{ad}/kT). \quad (3)$$

Here k is the Boltzman constant and T-temperature. Values of 0.55 eV have been obtained for the SiO_x and CdSe single layers; for GeS_2 E_{ad}=0.85 eV. The extremely low (~4.10^{-9} $cm^2/V.s$) electron mobility in thermally evaporated SiO_x films and the much higher one (>100 $cm^2/V.s$) in polycrystalline CdSe layers imply that in the regular multilayer structures carrier transport in direction parallel to the layer plane should be along CdSe sublayers. The values of the dark conductivity σ_d (calculated assuming charge transport via CdSe sublayers only) and E_{ad} (related to the CdSe sublayers) obtained for the multilayer samples are shown in Table 1. It is seen that the ML conductivity is considerably lower (10^2-10^3 times) than that of CdSe single layers but 10-500 times higher than the conductivity of the SiO_x single layers. Moreover, in both SiO_x/CdSe and GeS_2/CdSe MLs (Tables 1 and 2), E_{ad} exhibits a non-monotonous change with sublayer thickness, however in all MLs it remains higher than that of CdSe single layers.

As shown above, in SiO_x-CdSe and GeS_2-CdSe composite films CdSe sublayers consist of nanoparticles, some of which contact each other and, most likely, form a nanoparticle network. We assumed that in the composite films carrier transport is mainly through this network [50]. The assumption was verified by dark current measurements carried out in direction perpendicular to the plane of SiO_x-CdSe CFs, deposited on polished aluminum substrates. In this case, carrier transport crosses the thick SiO_x "sublayers" and the measured ratio of parallel to perpendicular conductivity was >10^2. It should be noticed that the dark current activation energy in SiO_x-CdSe CFs gradually increases with decreasing CdSe nominal thickness, while in GeS_2-CdSe composite films E_{ad} exhibits a non-monotonous change with sublayer thickness. A weak dark current temperature dependence is observed in poly- and nanocrystalline layers, when carrier transfer from one particle to the next is realized either by tunneling through energetic barriers between microcrystals or by space-charge-limited currents. The observed strong dark current temperature dependences indicate that none of these transport mechanisms takes place in the SiO_x-CdSe multilayer structures. In accordance with the model developed for carrier transport in polycrystalline semiconductors [51], we consider that carrier transport in CdSe nanoparticle layers in both MLs and CFs is through a percolation level in the conduction band of CdSe nanoparticles. In this case, dark current activation is high because it is a sum of the Fermi-energy E_F in microcrystals and the height of the interface potential barriers E_b i.e. $E_{ad}=E_F+E_b$. In CdSe sublayers these barriers may be die to the observed random orientation of the NCs, which induces a great number of stacking defects at the CdSe-CdSe interfaces. In the framework of this model, the observed decrease in ML conductivity with decreasing sublayer thickness may be related to the increase of interface-to-volume ratio in CdSe NCs. Due to the up bending of the conduction band, a gradual E_F increase could be anticipated, which explans why the E_{ad} values measured in MLs are higher than those of the CdSe single layers. The non-monotonous E_{ad} change may be assigned to some fluctuations in the barrier height connected with either the annealing procedure or some other uncontrolled variations in the preparation conditions. An extremely high dark current activation energy has been obtained (Table 2) in the GeS_2/CdSe multilayers with thinnest sublayers, which were deposited in one step. It may be related to large barrier heights between CdSe nanoparticles created by the interruption of both sublayers.

It is interesting to note that, though the CdSe NC networks in the CFs is not so densely packed as that in MLs, the average parallel dark conductivity of the SiO_x-CdSe composite films, calculated adopting electron transport through the CdSe nanoparticle network, is much higher than the conductivity of the single SiO_x, CdSe layers and corresponding MLs (Table 1). Moreover, the dark current activation energy of the films having great CdSe nominal thickness is lower than that of the CdSe single layers and increases when nominal CdSe thickness decreases. This observation has been related [50] to the fact that the evaporation of an SiO_x layer onto a CdSe films produces an accumulation layer at the SiO_x-CdSe interface, thus causing a Fermi-level shift up in the interface region of the CdSe nanocrystals embedded in a SiO_x matrix. Since these NCs are very small, the SiO_x–induced accumulation layer, most likely, occupies the entire volume of each CdSe NC. The low dark current activation energy E_{ad} measured in the large NCs implies that, due to accumulation effect of SiO_x, the potential barriers for electrons at the CdSe-CdSe NC contact interfaces should be very

low i.e. $E_{ad} = E_F + E_b \approx E_F$. On the other hand, a size-induced increase in the optical band gap of CdSe NCs has been observed [3], which causes a quantum-size shift up of the CdSe conduction band bottom. In fact, in samples having CdSe nominal thickness of 4.0 and 6.0 nm, $E_{ad} \approx E_F$ is smaller than that of CdSe single layers, which is an indication of a significant upward shift of the Fermi-level due to the accumulation effect of SiO_x. The observed conductivity decrease and E_{ad} increase when decreasing NC size below 5 nm (Table 1) is, most likely, due to a great size-induced shift up of the conduction band bottom, not compensated by the accumulation effect of the SiO_x matrix. Such an accumulation effect has not been observed in GeS_2-CdSe CFs, in which E_{ad} remains higher (Table 2) and the dark conductivity is lower than that of CdSe single layers for all nominal sublayer thicknesses.

Table 2. Experimental parameters for as-deposited GeS_2 and CdSe single layers and GeS_2 - CdSe multilayer structures prepared at the same deposition conditions.

	Regular multilayers	Composite films
Nominal CdSe sublayer thickness d_w (nm)	Dark current activation energy, E_{ad} (eV)	Dark current activation energy, E_{ad} (eV)
GeS_2 (1000)	0.85	
CdSe (200)	0.55	
10.0	0.76	
5.0	0.65	0.60
4.0	0.76	
3.0		0.71
2.5	0.68	
2.5*	1.05*	
2.0		0.58
1.0		0.86

*Multilayers in which each sublayer was deposited in one step.

In order to obtain information about the height of the CdSe-CdSe interface barriers in SiO_x/CdSe MLs, we measured [50] temperature dependencies of the photocurrent parallel to the layer plane under white light illumination and T>290 K. The photocurrent in polycrystalline films is described by the relation [51]

$$I_p = I_{po}\exp(-E_{ap}/kT) = eFG\mu_D\tau. \qquad (4)$$

Here E_{ap}-photocurrent activation energy, e-electron charge, F-applied electric field, G-carrier generation rate, $\mu_D = \mu_{Do}\exp(-E_b/kT)$-carrier drift mobility and τ-carrier lifetime. The obtained E_{ap} values are show in Table 1. In disordered semiconductors [52] the temperature dependence of carrier lifetime is much weaker than that of the drift mobility, and then $E_{ap} \approx E_b$. The parallel E_{ap} (E_b) and E_{ad} change observed (Table 1) supports the above assumption that some variations in the barrier height are responsible for the observed non-monotonous E_{ad} change in MLs. The last result also indicates that the E_b value is rather low (< 0.25 eV) and for this reason significant three-dimensional electron and phonon confinement was not observed in CdSe sublayes of MLs [40].

Spectral photocurrent measurements have been widely used in order to measure thin film absorption at energies around and below their optical band gap with accuracy higher than that of the transmission-reflection measurements [53,54]. The existence of percolation paths in the discontinuous CdSe layers made possible photocurrent measurements on SiO_x-CdSe [3] and GeS_2-CdSe CFs. The low CdSe total thickness in CFs (<100nm) allowed correct absorption measurements at energies higher than the optical band gap of CdSe nanoparticles, which revealed fine structure in the CFs absorption spectra. Such a structure, related to the great spin-orbit splitting in the valence band of CdSe and valence band mixing effects in strong carrier confinement regime, was not observed in the optical absorption spectra of $CdS_{1-x}Se_x$ doped glasses. The observed features in the absorption spectra of SiO_x-CdSe and GeS_2-CdSe CFs will be discussed in another work.

6. Conclusions

Fabrication of continuous and discontinuous CdSe nanoparticle layers during physical vapor deposition of CdSe on smooth and rough surface of amorphous SiO_x and GeS_2 has been described. It has been suggested that homogeneous embryo formation occurs at the first stage of CdSe deposition on the smooth surface; further CdSe deposition can lead to new embryo formation, gradual increase in the nanoparticle size and coalescence. On a rough surface there exist randomly distributed 'defect' points, at which embryo formation starts with preference. We assumed that, independently on the chemical nature of the surface, at the very beginning of CdSe deposition embryos are formed at those surface positions at which the curvature and lattice stress are the greatest. The relatively narrow nanocluster size distribution in CFs indicated that, most likely, further CdSe deposition does not create new embryos but leads mainly to an increase in the nanocluster size. Based on this nanoparticle growth mechanism, one can assume that semiconductor nanoparticle from various materials may be prepared on the rough surface of amorphous oxides and chalcogenides.

Acknowledgements

The author thanks Z. Levi and Dr. Z. Aneva, who took part in sample preparation and discussion of most results described in this article. She is also grateful to Dr. H.Hofmeister from the Max-Plank Institute, Halle, Germany for the high resolution electron microscopy measurements as well as to Assoc. Prof. M. Popescu from the National Institute of Material Physics, Bucharest, Romania for the SAXRD measurements carried out on SiO_x/CdSe multilayers.

References

[1] A. Ekimov, J. Lumin., **70**, 1 (1996).
[2] A. Gurevich, A. Ekimov, A. I. Kudryavtsev, O. G. Lyubinskaya, A. V. Osinskii, A. S. Usikov, N. N. Faleev, Sov. Phys. Semicond., **28**, 830 (1994).
[3] D. Nesheva, Z. Levi, Semicond. Sci. Technol., **12,** 1319 (1997).
[4] C. B. Murray, D. J. Norris, M. G. Bawendi, J. Am. Chem. Soc., **115**, 8706 (1993).
[5] J. E. Bowen Katari, V. L. Cilvin, A. P. Alivisatos, J. Phys. Chem., **98**, 4109 (1994).
[6] P. D. Persans, An Tu, Y. J. Wu, M. Lewis, J. Opt. Soc. Am., **B6,** 818 (1989).
[7] I. Ekimov, F. Hache, M. C. Schanne-Klein, D. Ricard, C. Flytzanis, I. A. Kudryavtsev, T. V. Yazeva, A. V. Rodina, Al. L. Efros, J. Opt .Soc. Am., **B10,** 100 (1993).
[8] R. K. Jain, R. C. Lind, 1983 J. Opt. Soc. Am., **73,** 647 (1983).
[9] P. Maly, F. Trojanek, A. Svoboda, J. Opt. Soc. Am., **B10,** 1890 (1993).
[10] A. Vanhaudenarde, M. Trespidi, R. Frey, J. Opt. Soc. Am., **B11,** 1474 (1994).
[11] F. Cerdeira, I. Torriani, P. Motisuke, V. Lemos, F. Decker, Appl. Phys., **A46,** 107 (1988).
[12] B. O. Dabbousi, M. B. Bawendi, O. Onitsuka, F. Rubner, Appl. Phys. Lett., **66,** 1316 (1995).
[13] K. Tsunemoto, A. Kawabuch, H. Kitayama, Y. Osaka, H. Nasu, Jap. J. Appl. Phys., **29**, 2481 (1990).
[14] N. F. Borrelli, D. W. Hall, H. J. Hollandy, D. W. Smith, J. Appl. Phys., **61**, 5399 (1987).
[15] T. Orii, Sh. Kaito, K. Matsuishi, S. Onari, T. Arai, J. Phys.: Condens. Matter, **9**, 4483 (1997).
[16] D. Tonova, M. Patrini, P. Tognini, A. Stella, P. Cheyssac, R. Kofman, J. Phys.: Condens. Matter, **11,** 2211 (1999).
[17] T. P. Drüsedau, A. N. Panckow, F. Klabunde, J. Non-Cryst. Solids, **198-200**, 829 (1996).
[18] D. Babonneau, F. Petroff. J.L. Maurice, F. Fettar, A. Vaures, A. Naudon, Appl. Phys. Lett, **76,** 2892 (2000).
[19] B. P. Zhang, T. Yasuda, Y. Segawa, H. Yaguchi, K. Onabe, E. Edamatsu, T. Itoh, Appl. Phys. Lett., **70**, 2413 (1997).
[20] I. Honma, H. Komiyama, K. Tanaka, Phil. Mag., **60**, 3 (1989).
[21] G. V. M. Williams, A. Bittar,. H. J. Trodahl, J. Appl. Phys., **67**, 1874 (1990).
[22] I. Honma, H. Hotta, H. Komiyama, K. Tanaka, J. Non-Cryst. Solids, **97-98**, 947 (1987).
[23] P. V. Santos, M. Hundhausen, L. Ley, C. Viczian, J. Appl. Phys., **69**, 778 (1991).

[24] E. Vateva, D. Nesheva, J. Non-Cryst. Solids, **191,** 205 (1995).
[25] D. Nesheva, E. Vateva, Z. Levi, D. Arsova, Phil. Mag., **B72**, 67 (1995).
[26] D. Nesheva, I. P. Kotsalas, C. Raptis, E. Vateva, J. Non-Cryst. Solids, **224,** 283 (1998).
[27] M. Popescu, F. Sava, A. Lorinczi, E. Vateva, D. Nesheva, P. J. Koch, T. Gutberlet, W. Uebach, H. Bradaczeck, Solid State Commun., **103,** 431 (1997).
[28] H. Xu, Y. Wang, G. Chen, Phys. Stat. Solidi (a), **143**, K87 (1994).
[29] P. Wickboldt, D. Pang, J. H. Chen, H. M. Cheong, W. Paul, J. Non-Cryst. Solids, **198-200**, 813 (1996).
[30] K. J. Chen, J. G. Jiang, X. F. Huang, Z. F. Li, X. X. Qu, J. Non-Cryst. Solids, **164-166**, 853 (1993).
[31] X. Huang, Zh. Li, W. Wu, K. Chen, X. Chen, Zh. Liu, J. Non-Cryst. Solids, **198-200**, 821 (1996).
[32] Z. Zhang, R. Cheng, H. Fritzsche, J. Non-Cryst. Solids, **97-98**, 923 (1987).
[33] R. Ionov, D. Nesheva, Thin Solid Films, **213**, 230 (1992).
[34] E. Vateva, Proc. NATO Advanced Research Workshop, Kishinau, Moldova, Eds. A. Andriesh, M. Bertolotti, Kluwer Academic Publishers, Netherlands, p. 61, (1996).
[35] E. Vateva, G. Tschaushev, J. Optoel. Adv. Matterials, **1**, No2, 9 (1999).
[36] E. Vateva, R. Ionov, D. Nesheva, D. Arsova, Phys. Status Solidi (a), **128**, K23 (1991).
[37] M. Popescu, F. Sava, E. Lorinczi, E. Vateva, D. Nesheva, G. Tschaushev, I. N. Mihailescu, P. J. Koch, S. Obst, H. Bradaczeck, Proc. SPIE, **3409**, 964 (1998).
[38] D. Nesheva, J. Optoel. Adv. Matterials, **1**, No3, 13 (1999).
[39] K. L. Chopra, Electrical phenomena in thin films, Mir, Moskwa, (1972).
[40] D. Nesheva, C. Raptis, Z. Levi, Phys. Rev., **B58**, 7913 (1998).
[41] D. Nesheva, H. Hofmeister, Solid State Commun., **114**, 511 (2000).
[42] D. Nesheva, H. Hofmeister, Z. Levi, Z. Aneva, to be published
[43] D. Nesheva, H. Hofmeister, Z. Levi, Z. Aneva, J. Phys.: Condens. Matt., **12**, 751 (2000).
[44] S. Sen, S. K. Halder, S. P. S. Gupta, J. Phys. Soc. Jpn., **38,** 1641 (1975).
[45] M. Gusso, L. De Caro, L. Tapfer, Solid State Commun., **101,** 665 (1997).
[46] O. Lublinskaya, S. Gurevich, A. Ekimov, I. Kudryavtsev, A. Osinskii, M. Gandais, Y. Wang, J. Cryst. Growth, **184-185**, 360 (1998).
[47] M. Zacharias, J. Bläsing, J. Christen, U. Wendt, J. Non-Cryst. Solids, **198-200,** 919 (1996).
[48] C. T. Campbell, Surf. Sci. Rep., **27**, 1 (1997).
[49] J. Tersoff, Yu. Tu, G. Grinstein, Appl. Phis. Lett., **73**, 2328 (1998).
[50] D. Nesheva, Z. Levi, V. Pamukchieva, J. Phys.: Condens. Matt., **12**, 3967 (2000).
[51] L. L. Kazmerski, Polycrystalline and amorphous thin films and devices, Ed. L.L.Kazmerski, Academic Press, New York, (1980), chapter 3.
[52] N. F. Mott, E. A. Davis, Electron Processes in Non-Crystalline Materials, Clarendon Press, Oxford, 1979.
[53] G. Moddel, D. Anderson, W. Paul, Phys. Rev., **B22,** 1918 (1980).
[54] M. Vanecek, J. Kocka, J. Stuchlik, Z. Ozisek, O. Stika, A. Triska, Solar Energy Mater., **8,** 411 (1983).